Voltage boost effects in two-step photon upconversion solar cells with a modulation-doped structure

Watanabe, Kohei
Asahi, Shigeo
Zhu, Yaxing
Kita, Takashi

(Citation)
Journal of Applied Physics,130(8):085701

(Issue Date)
2021-08-28

(Resource Type)
journal article

(Version)
Version of Record

Journal of Applied Physics ARTICLE scitation.org/journal/jap

Voltage boost effects in two-step photon upconversion solar cells with a modulation-doped structure

Cite as: J. Appl. Phys. **130**, 085701 (2021); doi: 10.1063/5.0058518
Submitted: 31 May 2021 · Accepted: 5 August 2021 ·
Published Online: 23 August 2021

Kohei Watanabe, Shigeo Asahi,[a] Yaxing Zhu, and Takashi Kita

AFFILIATIONS

Department of Electrical and Electronic Engineering, Graduate School of Engineering, Kobe University, 1-1 Rokkodai, Nada, Kobe 657-8501, Japan

[a]**Author to whom correspondence should be addressed:** asahis@people.kobe-u.ac.jp

ABSTRACT

A two-step photon upconversion (TPU) solar cell is a single-junction solar cell with a suitably designed heterointerface in the intrinsic layer. At this interface, upconversion can take place by absorbing infrared light, which excites carriers to energies above the heterojunction barrier, and then an electric field extracts these upconverted carriers to the barrier material. In this work, we study this photoabsorption process in a TPU solar cell with a modulation-doped structure. The modulation doping technique enables us to control the electric field at the heterointerface, and we demonstrate that the efficiency of the TPU process strongly depends on the electric field at the heterointerface. While we show that the TPU process induced by infrared light leads to a significant increase in the external quantum efficiency, we also note that this TPU process is an adiabatic process. It is shown that the adiabatic intraband photoexcitation at the heterointerface is able to increase the open-circuit voltage even above the open-circuit voltage that we predict from the diode equation and the actual current increase. We demonstrate obvious voltage boost effects and elucidate the relationship between the current and voltage.

I. INTRODUCTION

Methods for electricity generation that use solar energy, such as photovoltaics, have attracted much interest as they can be used to cope with global environmental issues.[1–7] There are several cost factors for solar cells, and the solar cell conversion efficiency affects the power-generation cost while it also controls the footprint of the solar cell. The conversion efficiency of a solar cell is restricted mainly by photon transmission and carrier thermalization, and the theoretical efficiency limit that considers these two losses is approximately 31% under 1 sun illumination for a single-junction solar cell consisting of a single semiconductor.[8–10] To achieve higher efficiencies, it is necessary to reduce losses, for example, by combining different semiconductors with different bandgap energies to better match the absorption to the solar spectrum. The multi-junction solar cell is a promising architecture that achieves the current world record of the conversion efficiency, which is now approaching 50%. On the other hand, such a dramatic improvement in the efficiency is, in principle, also possible by using a single junction structure that contains a so-called intermediate band (IB) located at an appropriate energy level between the valence band (VB) maximum and the conduction band (CB) minimum of the host material. In this IB solar cell (IBSC) architecture,[11] conventional transitions occur from the VB to the CB and, simultaneously, the IB enables absorption of below-gap photons corresponding to transitions from the VB to the IB (interband transition) and from the IB to the CB (intraband transition). Such a cascaded two-step photoexcitation via the IB can achieve an adiabatic upconversion, which produces additional photocurrent with a marginal reduction of the output voltage in the ideal case.[11] The conversion efficiency of an ideal IBSC predicted by using the detailed balance model is 46.8% under 1 sun. This increase from the 18.5% at an output voltage of 1.98 V that would be provided by the host material if no IB was present is accompanied by a voltage reduction of 0.25 V.[10,11]

However, in many reported IBSC designs,[12–17] the intraband transition from the IB to the CB is very weak because of three factors: a weak oscillator strength that arises from the optical selection rule, a low electron density in the IB state due to the presence of fast recombination processes, and a low density of states of the IB.[12–14]

Moreover, a part of the excited electrons in the CB quickly relaxes to the IB,[18] and the electrons in the IB can also be thermally activated to the CB. To improve the effect of the two-step photon upconversion (TPU) process, the photon ratchet IBSC has recently been proposed.[19] In the photon ratchet IBSC, electrons that have been excited to the IB are quickly transferred to a so-called ratchet band, which is not radiatively coupled with the VB and thus the electrons in the ratchet band have a long lifetime. In contrast to the IBSC, the initial state for the second excitation step to the CB is not the IB but the ratchet band.

We have recently proposed the so-called TPU solar cell (TPU-SC) architecture,[20–24] which is one practical example of implementing the ratchet concept. By using the detailed balance model, we estimated that the maximum conversion efficiency of the TPU-SC is 46.8% under 1 sun illumination at an output voltage of 1.73 V.[21] The TPU-SC is a single-junction solar cell with a heterointerface in the intrinsic layer. High-energy photons are absorbed in the wide-gap semiconductor (WGS) of the heterojunction, and photons with energies below the bandgap energy of the WGS are transmitted and can induce interband transitions in the narrow-gap semiconductor (NGS) of the heterojunction. The ratchet effect, i.e., the suppression of the recombination between excited electrons and holes in the VB, is achieved by the electric field in the intrinsic region: the electrons in the NGS CB drift to the heterointerface while the holes drift to the opposite direction. The electrons that have reached the interface are pumped upward to the WGS CB by absorbing additional below-gap photons; this is the intraband transition. The physics of GaAs/AlGaAs heterojunctions regarding use in photovoltaic cells has been investigated for a long time.[25–30] High-efficiency solar cells with low surface recombination velocities have been realized by using heterojunction structures as windows and back-surface field layers.[25–27] Furthermore, the generation of high-energy photons at such heterointerfaces with a large barrier has been extensively studied.[28–30] The TPU-SC concept is basically an extension of this phenomenon to realize an IBSC.

TPU can occur at a heterointerface because the accumulated electrons can be optically excited above the barrier in the CB.[31] However, we need to consider that the intraband transition of electrons in an ideal two-dimensional structure is forbidden for light at normal incidence.[32] Therefore, in our TPU-SC devices, an InAs QD layer is inserted at the heterointerface. The finite thickness of the accumulation layer relaxes the selection rule, and thus the InAs QDs are considered to enhance the TPU efficiency. It is well known that the electronic wavefunctions in QDs are quantized in all three dimensions, and light can induce intraband transitions irrespective of the polarization direction.[33] The electrons at the heterointerface obey the selection rule modified by the QDs and can be efficiently pumped into the CB of the barrier by infrared (IR) light.

An important feature is that the adiabatic intraband photoexcitation by additional IR light can also increase the voltage of a TPU-SC; we previously observed an IR-induced enhancement in both the photovoltage and the external quantum efficiency (EQE) in a TPU-SC based on a GaAs/$Al_{0.3}Ga_{0.7}As$ heterojunction.[20] In principle, this voltage boost effect due to TPU at the heterointerface can increase the open-circuit voltage of a TPU-SC even above the voltage corresponding to the NGS bandgap. Because the introduction of the WGS barrier necessarily reduces the photocurrent, a significant TPU-induced voltage boost, which improves the quasi-Fermi level separation, is important to exceed the ideal conversion efficiency of the single-junction solar cell. Furthermore, an additional enhancement in the photocurrent at reverse bias voltages has been found, which indicates that the photocurrent is influenced by the carrier extraction properties of upconverted electrons at the heterointerface.[23] In this work, we studied the effect of the electric field at the heterointerface on the TPU process in TPU-SCs. We prepared four samples with different local electric fields controlled by modulation doping in $Al_{0.3}Ga_{0.7}As$. We confirmed that the additional intraband excitation at the heterointerface due to IR light results in a dramatically improved EQE at room temperature. Furthermore, we measured the IR-induced changes in the short-circuit current and open-circuit voltage. Based on the difference between the experimentally observed changes and the theoretical changes calculated using the current–voltage (J–V) relationship and a local ideality factor, we found that the photocurrent increase due to the adiabatic photoexcitation process also boosts the voltage.

II. EXPERIMENT

A. Modulation-doped TPU-SCs

We fabricated three types of TPU-SCs and an additional reference TPU-SC without modulation doping. These TPU-SCs employ an n–i–p single-junction structure where the heterointerface of the $Al_{0.3}Ga_{0.7}As$/GaAs heterojunction lies in the intrinsic layer. Here, $Al_{0.3}Ga_{0.7}As$ and GaAs correspond to the WGS and NGS materials, respectively. The difference between the samples was the degree of modulation doping in the $Al_{0.3}Ga_{0.7}As$ layer. Table I summarizes the growth details of the four TPU-SCs. A brief description of the device fabrication is provided below.

Each TPU-SC was fabricated on a p^+-GaAs (001) substrate by solid-source molecular beam epitaxy. First, a 150-nm-thick p-GaAs (Be: $2.0 \times 10^{18}/cm^3$) layer was grown on a p^+-GaAs (Be: $1.0 \times 10^{19}/cm^3$) buffer layer with a thickness of 400 nm at a substrate temperature of 550 °C. Then, we deposited the intrinsic region consisting of a 1140-nm-thick i-GaAs, an InAs QD layer, and a GaAs capping layer with 10 nm thickness. The nominal thickness of the InAs layer was 0.64 nm (2.1 monolayers), which is thick enough to induce QD formation via the Stranski–Krastanov growth mode. The QDs had a typical height and width of 3 and 20 nm, respectively, and the QD density was approximately $1.0 \times 10^{10}\ cm^{-2}$.[34] The substrate temperature before the InAs QD growth was 550 °C. The InAs QDs and the GaAs capping layer were grown at 490 °C. Subsequently, for the modulation-doped structure, first, an i-$Al_{0.3}Ga_{0.7}As$ layer and then an n-$Al_{0.3}Ga_{0.7}As$ layer were grown on the GaAs capping layer at 500 °C. The total thickness of this $Al_{0.3}Ga_{0.7}As$ region was 250 nm and each device was prepared with a different thickness of the n-$Al_{0.3}Ga_{0.7}As$ layer (Table I; 0, 120, 180, and 240 nm). Finally, a 150-nm-thick n-$Al_{0.3}Ga_{0.7}As$ (Si: $1.0 \times 10^{17}\ cm^{-3}$) layer, a 30-nm-thick n^+-$Al_{0.3}Ga_{0.7}As$ (Si: $2.5 \times 10^{17}\ cm^{-3}$), and a contact layer ($n^+$-GaAs with a Si doping concentration of $2.5 \times 10^{18}\ cm^{-3}$ and a thickness of 50 nm) were grown at 500 °C. To perform the J–V measurements, electrodes were deposited on the top and bottom surfaces (we used metal contacts consisting of Au/Au–Ge and Au/Au–Zn, respectively). For the top

TABLE I. Details of the TPU-SC structures grown by molecular beam epitaxy. The predicted electric field strengths at the heterointerface are provided in the first row. The reference TPU-SC (with an electric field of 11.0 kV/cm) was prepared without modulation doping. The other three devices are modulation-doped TPU-SCs.

	TPU-SC with 11.0 kV/cm		TPU-SC with 123 kV/cm		TPU-SC with 16.6 kV/cm		TPU-SC with 322 kV/cm	
	Thickness (nm)	Carrier concentration (cm^{-3})	Thickness (nm)	Carrier concentration (cm^{-3})	Thickness (nm)	Carrier concentration (cm^{-3})	Thickness (nm)	Carrier concentration (cm^{-3})
n+−GaAs	50	2.5×10^{18}	50	2.5×10^{18}	50	2.5×10^{18}	50	2.5×10^{18}
n+−$A1_{0.3}Ga_{0.7}As$	30	2.5×10^{17}	30	2.5×10^{17}	30	$2.5 \times l0^{17}$	30	2.5×10^{17}
n-$A1_{0.3}Ga_{07}As$	150	1.0×10^{17}	150	1.0×10^{17}	150	1.0×10^{17}	150	1.0×10^{17}
n-$A1_{0.3}Ga_{07}As$	…	…	120	1.0×10^{16}	180	1.5×10^{16}	240	3.0×10^{16}
i-$A1_{0.3}Ga_{0.7}As$	250	…	130	…	70	…	10	…
InAs-QD layer	InAs: 0.64 nm (2.1 ML), GaAs capping layer thickness: 10 nm							
i-GaAs	1140	…	1140	…	1140	…	1140	…
p-GaAs	150	2.0×10^{18}	150	2.0×10^{18}	150	2.0×10^{18}	150	2.0×10^{18}
p^+-GaAs	400	1.0×10^{19}	400	1.0×10^{19}	400	1.0×10^{19}	400	1.0×10^{19}

electrode, we used a comb pattern in which the spacing between the 0.25-mm-thick grid fingers is 0.45 mm. The dimensions of the final devices were 4.0×3.8 mm^2.

Figures 1(a) and 1(b) show the approximate band structures and the electric field distributions in the region around the heterointerface, respectively. These curves were obtained by theoretical simulations of the four devices without considering the InAs QDs. We employed the software nextnano3, and we used the default values in the nextnano3 material database.[35,36] The default values of the material parameters are those listed in Ref. 37. The electric field strengths at the heterointerface lie in the range from 11.0 to 32.2 kV/cm, and it can be confirmed that the electric field at the heterointerface increases with the modulation doping concentration. Therefore, we expect that the carrier extraction efficiency of upconverted electrons can be improved by selecting a suitable modulation-doped structure.

B. External quantum efficiency measurements

To investigate the photocurrent generation efficiency, we measured the EQE under short-circuit conditions at room temperature. For the measurement of the EQE spectrum, light of a tungsten halogen lamp was passed through a 140-mm single monochromator and chopped by an optical chopper with a frequency of 800 Hz to enable photocurrent detection using a lock-in technique. The monochromatic excitation light intensity varied with wavelength (we confirmed a variation in the range of 17–32 $\mu W/cm^2$, and the total power density of the tungsten halogen lamp in the wavelength range of 640–1100 nm was approximately 4 mW/cm^2). We also characterized the change in the EQE spectrum that is induced by additional IR light irradiation from a continuous-wave (cw) laser at a wavelength of 1319 nm. The beam diameter of this light at 1319 nm was 1.2 mm, and the excitation power density was 90 mW/cm^2. Note that the wavelength of the IR light is too long to induce interband transitions in GaAs. The measured EQE and the change in the EQE due to additional IR-light irradiation are denoted by η_Q and $\Delta\eta_Q$, respectively. The effect of the IR light is briefly discussed below.

When the $Al_{0.3}Ga_{0.7}As$ layer is excited, the photogenerated electrons and holes are simply collected at their corresponding electrodes. On the other hand, photons whose energy is lower than the bandgap of $Al_{0.3}Ga_{0.7}As$, predominantly generate electrons and holes in the intrinsic GaAs layer. While the holes drift toward the *p*-layer of GaAs, the electrons drift toward the opposite side. However, these electrons are partially obstructed by the CB offset at the heterointerface. The electrons that have reached the interface can be pumped upward into the $Al_{0.3}Ga_{0.7}As$ barrier by absorbing low-energy photons such as those provided by the IR excitation source.

C. IR-induced changes in the current–voltage characteristics

To elucidate the effects of the electric field at the heterointerface, we also measured the IR-induced changes in the *J*–*V* characteristics as functions of the interband and intraband excitation power densities. In these measurements, a cw Ti:sapphire laser with a wavelength of 800 nm was used for the interband excitation in GaAs. The cw IR laser with a wavelength of 1319 nm was used to pump electrons accumulated at the heterointerface upward to the $Al_{0.3}Ga_{0.7}As$ barrier. This corresponds to the intraband excitation. The beam diameter of the Ti:sapphire laser was about 1.1 mm. To identify the different contributions, we define ΔJ_{SC} and ΔV_{OC} as the changes in the short-circuit current and the open-circuit voltage that occur when the IR light irradiates the sample in addition to the 800-nm light, respectively. First, we measured the ΔJ_{SC} and ΔV_{OC} values as a function of the interband excitation power density in the case of a constant IR excitation power density of 500 mW/cm^2. The interband excitation power density was changed from 0.02 to 500 mW/cm^2. Next, we fixed the interband excitation power density at 0.5 mW/cm^2 and measured the ΔJ_{SC} and ΔV_{OC} values of the moderately modulation-doped TPU-SC as a function of the intraband excitation power density. The latter was changed from 4 to 1000 mW/cm^2. The photocurrent and photovoltage were detected using a source measure unit (Keithley SourceMeter 2400). All measurements were conducted at room temperature.

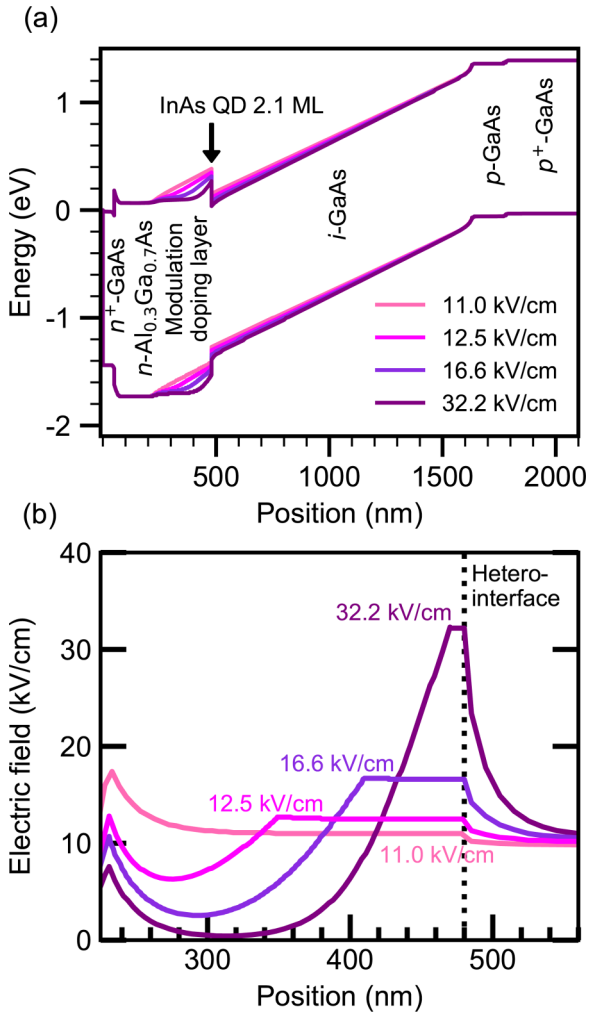

FIG. 1. (a) Band diagrams calculated for the TPU-SCs at a bias voltage of 0 V. These calculations do not take the InAs QDs into account, but in the actual devices, InAs/GaAs QD layers with a thickness equivalent to 2.1 monolayers are inserted 10 nm in front of the heterointerface. (b) Electric field distributions derived from (a) in the vicinity of the heterointerface. The electric field strengths at the heterointerface are indicated in the figure.

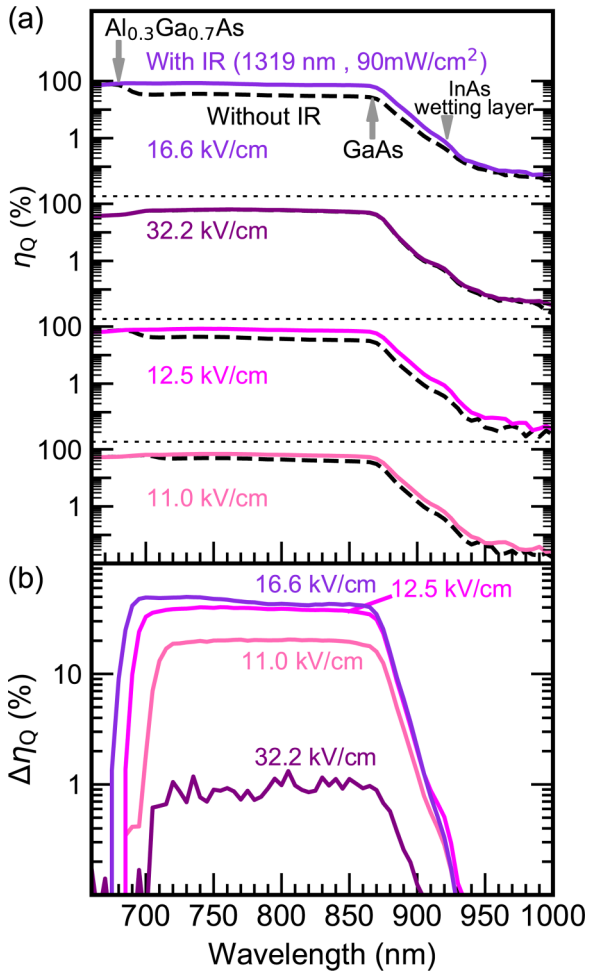

FIG. 2. (a) EQE spectra obtained from the four TPU-SCs under short-circuit conditions with (solid curves) and without (broken black curves) additional IR-light irradiation. The EQE measurements were conducted at room temperature. (b) IR-induced changes in the EQE ($\Delta\eta_Q$). The $\Delta\eta_Q$ values describe the difference between the EQE obtained with additional IR irradiation (1319 nm) and the EQE obtained without the IR light.

III. RESULTS AND DISCUSSION

A. External quantum efficiency spectra

Figure 2(a) shows the EQE spectra of the four TPU-SCs under short-circuit conditions. The solid curve was obtained using both the monochromatic light and the additional IR light for excitation. The black dashed curve was obtained without the additional IR light. In this latter curve, two clear absorption edges appear at 685 and 875 nm, which correspond to the bandgaps of $Al_{0.3}Ga_{0.7}As$ and GaAs, respectively. The small feature at 915 nm is assigned to the InAs wetting layer. The EQE for the direct excitation of $Al_{0.3}Ga_{0.7}As$ is relatively high because almost all photogenerated electrons and holes are collected by the corresponding electrodes. The photons with wavelengths between 685 and 875 nm generate carriers in GaAs via interband excitation. The drop in the EQE signal intensity in this wavelength range is attributed to the fact that the directly excited electrons in GaAs (which drift toward the front contact) are partially blocked by the $Al_{0.3}Ga_{0.7}As$ barrier. We consider that these electrons overcome the barrier via thermal excitation. Tunneling is only important for the sample with an electric field of 32.2 kV/cm at the heterointerface. On the other hand, the solid curves do not exhibit an absorption edge at 685 nm. The absorption edge at 685 nm disappears because the IR light pumps the accumulated electrons at the heterointerface upward to the $Al_{0.3}Ga_{0.7}As$ barrier. Note that there is almost no difference

between the EQE spectra with and without IR for the sample with 32.2 kV/cm at the heterointerface. This is attributed to the fact that the electrons can overcome the barrier efficiently by tunneling.

Figure 2(b) summarizes the IR-induced changes in the EQE spectra of the four TPS-SCs. These spectra were obtained by subtracting the EQE obtained without IR light from the EQE obtained with IR light for each device. $\Delta\eta_Q$ of the reference TPU-SC (electric field at the heterointerface: 11.0 kV/cm) is approximately 20% in the wavelength range from 700 to 870 nm. For the TPU-SCs with electric fields of 12.5 and 16.6 kV/cm at the heterointerface, the $\Delta\eta_Q$ values increase up to ≈38% and ≈45%, respectively. This increase in $\Delta\eta_Q$ by a factor of about 2 is explained by a better carrier separation and a better electron extraction at the interface: The modulation doping realizes a more efficient electron–hole separation in GaAs and thus higher electron densities can be realized at the heterointerface. As the intraband transition probability is proportional to the electron density of the initial state of the transition, a denser accumulation of electrons causes a more efficient intraband transition from the initial state to the final state above the CB edge of $Al_{0.3}Ga_{0.7}As$. Additionally, the modulation doping increases the electric field at the heterointerface, as shown in Fig. 1(b). The stronger electric field increases the yield of the extraction of the upconverted electrons from the final state of the intraband transition to the $Al_{0.3}Ga_{0.7}As$ barrier. However, we also note that the TPU-SC with an electric field of 32.2 kV/cm exhibits a considerably lower $\Delta\eta_Q$. This reduction in $\Delta\eta_Q$ indicates that a too strong electric field can give rise to severe tunneling escape of electrons at the heterointerface. Therefore, the density of the accumulated electrons at the interface decreases, which implies that $\Delta\eta_Q$ decreases while η_Q increases as shown in Fig. 3(a). According to these observations, 16.6 kV/cm is considered to be close to the optimum electric field for this type of TPU-SC.

B. Interband excitation power dependences of ΔJ_{SC} and ΔV_{OC}

Next, we studied the changes in the short-circuit current and open-circuit voltage caused by the TPU process as a function of the interband excitation power density P_{inter}. Figure 3(a) shows the P_{inter} dependences of the ΔJ_{SC} values obtained from the TPU-SCs with electric fields of 11.0, 16.6, and 32.2 kV/cm. To understand the significance of these curves for devices, the excitation power density is also provided in terms of equivalent suns with respect to the device structure (indicated in the upper horizontal axis): in our case, 1 sun corresponds to 20 mW/cm^2 for the interband excitation, since this is equivalent to the photon flux of the AM1.5G spectrum in the wavelength range from 685 ($Al_{0.3}Ga_{0.7}As$ bandgap energy) to 875 nm (GaAs bandgap energy). For the data in Fig. 3(a), the intraband excitation power density was fixed at 500 mW/cm^2, which corresponds to 18.5 suns. Here, 1 sun corresponds to 27 mW/cm^2 for the intraband excitation power density, since this is equivalent to the photon flux of the AM1.5G spectrum within the range 875–4000 nm. Note that the upper horizontal axis is only provided to clarify why the excitation intensities used in this work are considered to be relevant to devices. On the other hand, one should bear in mind that our excitation conditions differ from the actual operation under AM1.5G illumination, which is as broad spectrum ranging from the ultraviolet to the mid-IR region. Since a broadband illumination may have a significant effect, the presented photocurrent- and photovoltage-increases induced by the intraband excitation may differ from the values under AM1.5G illumination.

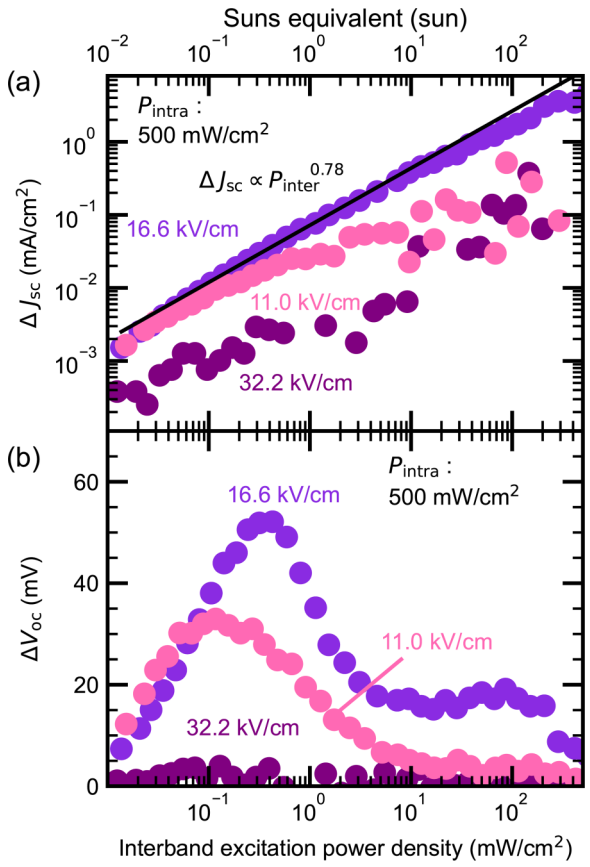

FIG. 3. (a) Interband-excitation power dependences of the IR-induced enhancement in the short-circuit current, ΔJ_{SC}. The data of the TPU-SCs with electric fields of 11.0 (the reference cell), 16.6, and 32.2 kV/cm at the heterointerface are shown. (b) Interband-excitation power density dependences of the IR-induced open-circuit voltage improvements (ΔV_{OC}) for the same samples as in (a). The intraband excitation power density was fixed at 500 mW/cm^2. The indicated electric field strengths correspond to the values at the heterointerface.

In Fig. 3(a), we see that, in all samples, ΔJ_{SC} increases with P_{inter} and exhibits a sub-linear dependence on P_{inter}. In other words, the exponent of the power law for ΔJ_{SC} of the TPU-SC with 16.6 kV/cm is 0.78, while ΔJ_{SC} trends of the TPU-SCs with 11.0 and 32.2 kV/cm have smaller exponents. To interpret this result, we need to consider that the electron density at the heterointerface increases with P_{inter} and that an increasing negative charge at the interface weakens the electric field at the heterointerface. A weaker electric field leads to an increase in the hole density at the heterointerface and, therefore, the electron–hole recombination rate increases, leading to a sub-linear dependence of ΔJ_{SC} on P_{inter}.[24]

ΔJ_{SC} of the TPU-SC with 16.6 kV/cm is larger than that of the reference TPU-SC because of the higher electron density at the interface and the better extraction efficiency of upconverted electrons as mentioned in the explanation of the EQE data. Furthermore, the TPU-SC with 32.2 kV/cm shows a low ΔJ_{SC} resulting from the tunneling leakage of electrons at strong electric fields.

Figure 3(b) shows the P_{inter} dependences of ΔV_{OC} for the three TPU-SCs investigated in Fig. 3(a). Each curve exhibits a peak at a certain interband excitation intensity P_{inter}. We find that the TPU-SC with 16.6 kV/cm has a higher ΔV_{OC} than the reference cell, and its ΔV_{OC} peak appears at a power density that is higher than P_{inter} for the ΔV_{OC} peak of the reference TPU-SC. Obviously, the TPU-SC with 32.2 kV/cm shows a low ΔV_{OC}.

We consider that the carrier extraction in the adiabatic TPU process at the heterointerface leads to an increase in the output voltage. In other words, compared to thermal excitation and tunneling, this IR-induced transport of electrons to the $Al_{0.3}Ga_{0.7}As$ layer induces a split between the quasi-Fermi-levels of the electrons in the $Al_{0.3}Ga_{0.7}As$ and GaAs layers. Figure 3(b) evidences that ΔV_{OC} increases with the interband excitation power density and exhibits a pronounced maximum at certain interband excitation intensity P_{inter}. To better understand the significance of these data, we compare the experimentally observed ΔV_{OC} with the theoretical $\Delta V'_{OC}$ calculated from the measured V_{OC}, short-circuit current (J_{SC}), and ΔJ_{SC}. We use the following equation, which is derived from the detailed balance model for a single-junction solar cell in the case of two-color excitation (see Appendixes A and B):

$$\Delta V'_{OC} = m\frac{k_b T}{q}\ln\left(\frac{\Delta J_{SC}}{J_{SC}+J_0}+1\right), \quad (1)$$

where k_b is the Boltzmann constant, T is the temperature of the solar cell, q is the elementary charge, J_0 is the reverse saturation current density, and m is the local ideality factor.[38] For J_0, we used the dark current density obtained at the reverse bias voltage where saturation occurs (and not the value corresponding to breakdown). For the estimation of m, we measured the voltage dependence of the dark current in the forward-bias region.[39] The dark J–V curves and the ideality factors are shown in Figs. 4(a) and 4(b), respectively. Theoretically, the diode ideality factor can assume values in the range 1–2.[40] However, in actual devices, factors larger than 2 can be observed due to unexpected losses, such as shunt and series resistances, and carrier trapping,[41–45] and even factors of up to 6.5 have been reported.[46–48] To evaluate the voltage boost, we employed Eq. (1) and considered the local ideality factor, which includes these above-mentioned unexpected losses. Figure 4(c) compares the experimentally observed ΔV_{OC} (closed circles) with the calculated $\Delta V'_{OC}$ values (dotted curves) for the TPU-SCs with 16.6 and 11.0 kV/cm. Both $\Delta V'_{OC}$ curves exhibit peaks, similar to the experimental results. The presence of these peaks can be explained using Eq. (1): At low interband excitation power densities, J_{SC} is much smaller than J_0, and the denominator in the logarithm is governed by J_0, resulting in an increase in $\Delta V'_{OC}$ with increasing ΔJ_{SC}. At

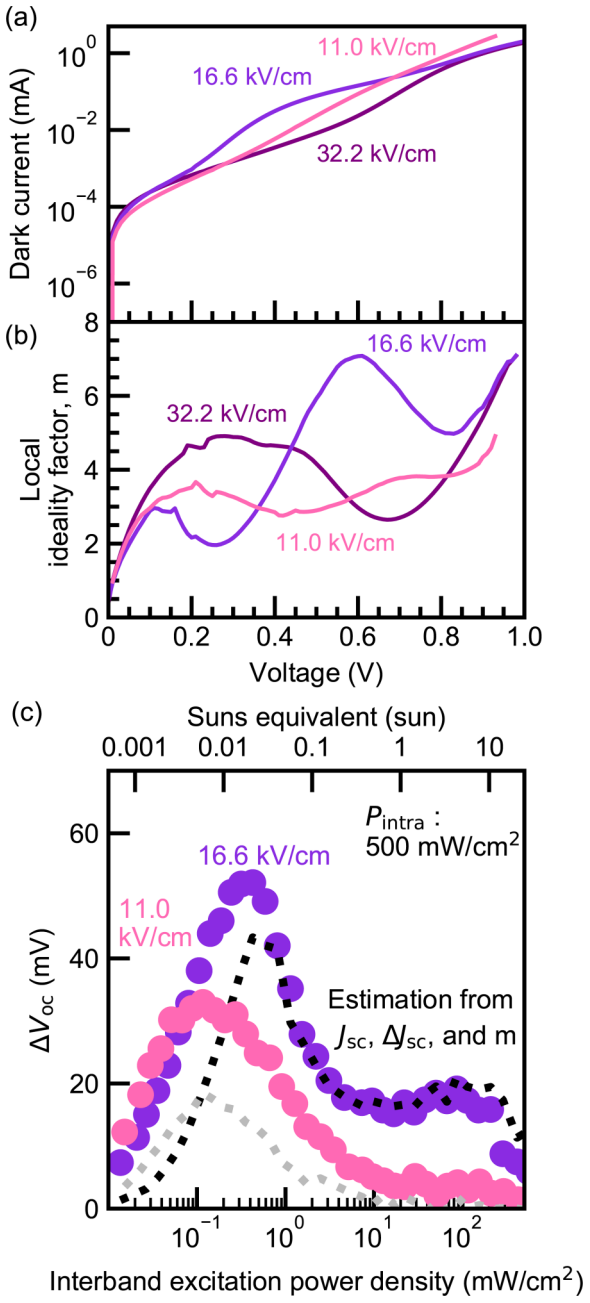

FIG. 4. (a) Dark I–V curves and (b) local ideality factors for the TPU-SCs with electric field strengths of 11.0, 16.6, and 32.2 kV/cm at the heterointerface. (c) The experimentally obtained ΔV_{OC} values are indicated by the closed circles, which are the same as in Fig. 3(b). The gray and black broken curves show the theoretical $\Delta V'_{OC}$ values calculated from the observed J_{SC} and ΔJ_{SC} values, and the local ideality factors for the TPU-SCs with 11.0 and 16.6 kV/cm, respectively. The diode ideality factors as a function of the interband excitation power density were calculated by using the relationship between the diode ideality factor and V_{OC} obtained without IR-light irradiation.

high interband excitation power densities, J_{SC} becomes much larger than J_0, and the denominator in the logarithm is governed by J_{SC}, which has a linear relationship with P_{inter}.[24] The linear relationship of J_{SC} and the sub-linear relationship of ΔJ_{SC} shown in Fig. 3(a) lead to a decrease in $\Delta V'_{OC}$ with P_{inter}.

Regarding the data in Fig. 4(c), it is important to note that the experimentally observed voltage increase exceeds the open-circuit voltage calculated from Eq. (1) and the local ideality factor. This deviation from the prediction is attributed to a voltage boost effect occurring at the heterointerface, i.e., the additional irradiation with IR light splits the quasi-Fermi levels at the heterointerface by the adiabatic TPU process.

We consider that the local ideality factors are a result of the device processing, which needs to be improved in future. For example, compared to theoretically estimated $\Delta V'_{OC}$ (broken curves), a significant ΔV_{OC} (solid circles) can be confirmed in the whole excitation range for the TPU-SC with 11.0 kV/cm, which exhibits a relatively low local ideality factor. These results suggest that an optimized electric field and optimized device processing can realize further improvements in the voltage boost effect.

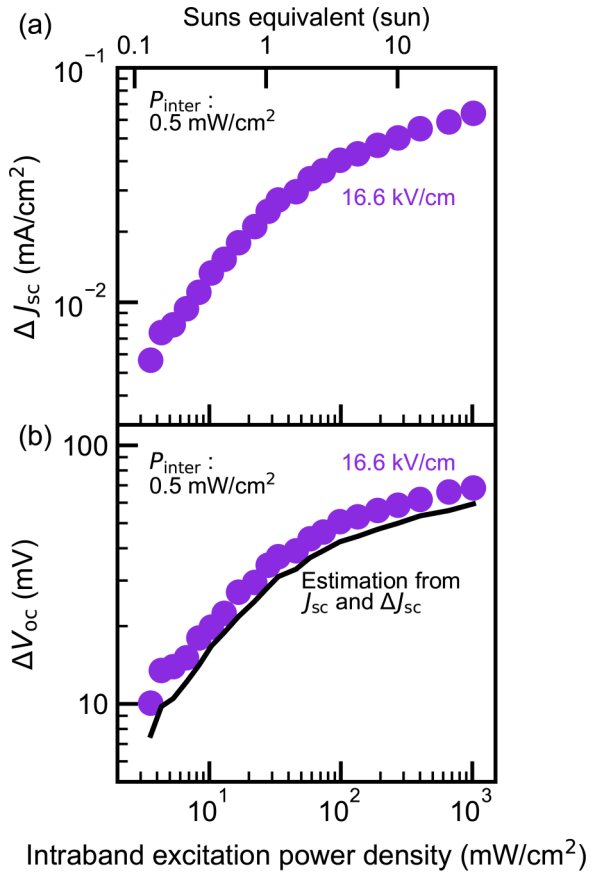

FIG. 5. The intraband-excitation power density dependences of (a) ΔJ_{SC} and (b) ΔV_{OC} of the modulation-doped TPU-SC with an electric field of 16.6 kV/cm at the heterointerface. The experimental ΔV_{OC} values are indicated by the purple dots, and the theoretical $\Delta V'_{OC}$ calculated from the observed J_{SC} and ΔJ_{SC} is shown by the black curve. The ideality factor is constant because the interband excitation power density is constant. The interband excitation power density was 0.5 mW/cm^2, which corresponds to the ΔV_{OC} peak position in Fig. 4(b).

C. Intraband-excitation power dependences of ΔJ_{SC} and ΔV_{OC}

The intraband-excitation power dependences of ΔJ_{SC} and ΔV_{OC} for the TPU-SC with 16.6 kV/cm are shown in Figs. 5(a) and 5(b), respectively. In these measurements, we fixed P_{inter} at 0.5 mW/cm^2, which is the excitation power density where the peak of ΔV_{OC} was observed in Fig. 4(c).

In Fig. 5(a), we can confirm that ΔJ_{SC} obeys a sub-linear relationship, because a stronger IR light can excite a larger fraction of the accumulated electrons, and thus the current improvement tends to saturate. When P_{inter} is increased, the resulting increase in the electron density pushes this saturation level up.

Figure 5(b) shows the dependence of ΔV_{OC} on the intraband excitation power density. The $\Delta V'_{OC}$ calculated using Eq. (1) is indicated by the solid curve. For this calculation, we used $V_{OC} = 110$ mV and $m = 3.0$. We find that ΔV_{OC} monotonically increases, which indicates that the adiabatic TPU process can be enhanced with the intraband excitation power density. The observed ΔV_{OC} surpasses the calculated $\Delta V'_{OC}$ in the entire measurement range, suggesting that this is a voltage boost effect caused by the TPU process.

IV. CONCLUSION

We have discussed the intraband absorption and carrier extraction process at the heterointerface in a TPU-SC. To study these processes, we used modulation doping to prepare devices with different electric field strengths and investigated their TPU properties. The change in the EQE, $\Delta\eta_Q$, exhibited a maximum for the TPU-SC with an electric field of 16.6 kV/cm and the obtained $\Delta\eta_Q$ was more than two times larger than that of the TPU-SC without modulation doping. The IR-induced short-circuit current increase, ΔJ_{SC}, of this modulation-doped TPU-SC monotonically increased with the interband and intraband excitation power densities. ΔV_{OC} of this device exhibited its maximum at a relatively low interband excitation power density and the peak value was larger than that of the TPU-SC without modulation doping. We observed a voltage boost effect due to the TPU process, that is, the actually observed IR-induced open-circuit voltage increase (ΔV_{OC}) is larger than the theoretical $\Delta V'_{OC}$ calculated from the measured short-circuit current (ΔJ_{SC}) and the local ideality factor, m. We have explained that this voltage boost effect is a result of the split of quasi-Fermi levels at the heterointerface by the adiabatic TPU process. Moreover, this ΔV_{OC} monotonically increased with the intraband excitation power density. The observed increase in J_{SC} and V_{OC} indicates that controlling the electric field at the heterointerface can improve the carrier extraction of upconverted electrons, and an optimum electric field (achieved, for example, by modulation doping) is essential for a highly efficient TPU process.

ACKNOWLEDGMENTS

This work was supported by the Japan Society for the Promotion of Science (JSPS) KAKENHI Grant Nos. JP18KK0145, JP19H00768, JP20K21004, and JP20K14792.

APPENDIX A: DERIVATION OF THE EQUATION OF ΔV_{OC}

To estimate the IR-induced voltage increase that can be expected from the current increase, $\Delta V'_{OC}$, we used the equation that describes V_{OC} of a conventional single-junction solar cell

$$V_{OC} = m\frac{k_b T}{q}\ln\left(\frac{J_{SC}}{J_0}+1\right), \tag{A1}$$

where k_b is the Boltzmann constant, T is the temperature of the solar cell, q is the elementary charge, J_0 is the reverse saturation current density, and m is the local ideality factor. The open-circuit voltage under a two-color photoexcitation condition can be divided into the open-circuit voltage due to single-color excitation, $V_{OC,single}$ and the open-circuit voltage change due to the additional IR irradiation, $\Delta V'_{OC}$. Similarly, J_{SC} can be divided into $J_{SC,single}$ and IR-induced ΔJ_{SC},

$$\begin{aligned}\Delta V'_{OC} &= m\frac{k_b T}{q}\ln\left(\frac{J_{SC}+\Delta J_{SC}}{J_0}+1\right) - m\frac{k_b T}{q}\ln\left(\frac{J_{SC}}{J_0}+1\right)\\ &= m\frac{k_b T}{q}\ln\left(\frac{\Delta J_{SC}}{J_{SC}+J_0}+1\right).\end{aligned} \tag{A2}$$

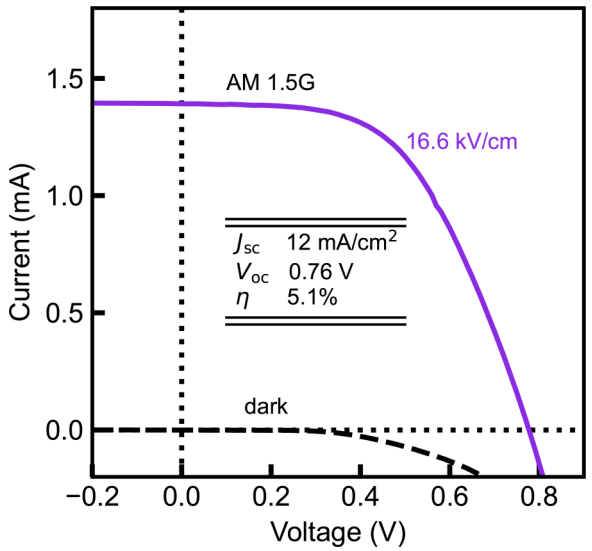

FIG. 6. Current–voltage characteristic of the TPU-SC with 16.6 kV/cm in the dark (black curve) and that under 1 sun AM1.5G illumination (purple curve). J_{SC}, V_{OC}, and the conversion efficiency η of this device are provided in the figure.

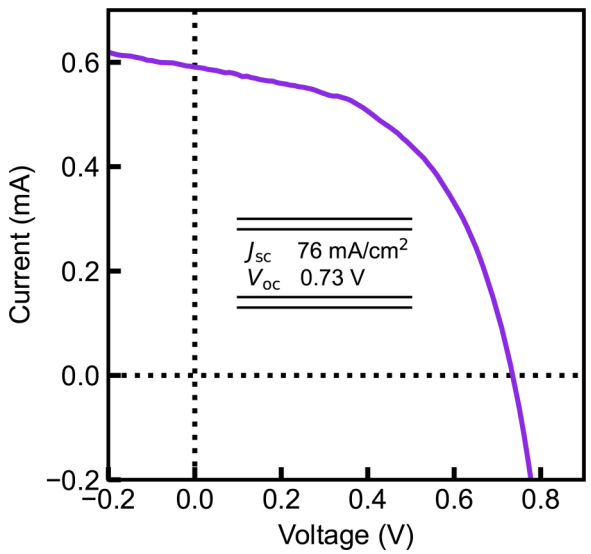

FIG. 7. Current–voltage characteristic of the TPU-SC with 16.6 kV/cm under the irradiation of the 800-nm laser with the power density of 807 mW/cm^2.

APPENDIX B: *J–V* CHARACTERISTICS

Figure 6 shows the *J–V* characteristic of the TPU-SC with an electric field of 16.6 kV/cm under 1 sun AM1.5G illumination and that in the dark. The obtained values of J_{SC}, V_{OC}, and η were 12 mA/cm^2, 0.76 V, and 5.1%, respectively. The efficiency is smaller than the value predicted by the detailed balance model,[9] showing that the further improvement of the device fabrication is required. Figure 7 also shows the *J–V* characteristic of the TPU-SC with the electric field of 16.6 kV/cm under the irradiation of the 800-nm laser with the power density of 807 mW/cm^2. Typical values of J_{SC} and V_{OC} were 76 mA/cm^2 and 0.73 V, respectively. The photocurrent under AM1.5G illumination shown in Fig. 6 exhibits almost constant in the voltage region less than ~0.35 V. In contrast to the *J–V* curve line shape in Fig. 6, photocurrent under the irradiation of the monotonic 800-nm light shown in Fig. 7 decreases with positively increasing voltage in the entire voltage region. Since the 800-nm laser selectively illuminates GaAs of the TPU-SC, all carriers are generated in the GaAs layer. Therefore, the observed photocurrent is only generated by the thermal and tunneling processes at the heterointerface. The number of extracted electrons sensitively depends on the internal electric field near the heterointerface and, therefore, decreases as the voltage positively increases.

DATA AVAILABILITY

The data that support the findings of this study are available from the corresponding author upon reasonable request.

REFERENCES

[1] A. De Vos, J. Phys. D: Appl. Phys. **13**, 839 (1980).
[2] N. Ekins-Daukes, Sol. Energy Mater. Sol. Cells **68**, 71 (2001).

[3]R. T. Ross and A. J. Nozik, J. Appl. Phys. **53**, 3813 (1982).
[4]M. A. Green, Prog. Photovoltaics Res. Appl. **9**, 123 (2001).
[5]M. A. Green, K. Emery, Y. Hishikawa, W. Warta, E. D. Dunlop, D. H. Levi, and A. W. Y. Ho-Baillie, Prog. Photovolt Res. Appl. **25**, 3 (2017).
[6]Y. Okada, N. J. Ekins-Daukes, T. Kita, R. Tamaki, M. Yoshida, A. Pusch, O. Hess, C. C. Phillips, D. J. Farrell, K. Yoshida, N. Ahsan, Y. Shoji, T. Sogabe, and J.-F. Guillemoles, Appl. Phys. Rev. **2**, 021302 (2015).
[7]R. Y. Lin, *Advanced Solar Power Technology-Multiple Junction Photovoltaics* (Springer Singapore, Singapore, 2020).
[8]L. C. Hirst and N. J. Ekins-daukes, Prog. Photovoltaics Res. Appl. **19**, 286 (2011).
[9]W. Shockley and H. J. Queisser, J. Appl. Phys. **32**, 510 (1961).
[10]T. Kita, Y. Harada, and S. Asahi, *Energy Conversion Efficiency of Solar Cells* (Springer Singapore, Singapore, 2019).
[11]A. Luque and A. Martí, Phys. Rev. Lett. **78**, 5014 (1997).
[12]A. Martí, E. Antolín, C. R. Stanley, C. D. Farmer, N. López, P. Díaz, E. Cánovas, P. G. Linares, and A. Luque, Phys. Rev. Lett. **97**, 247701 (2006).
[13]Y. Okada, T. Morioka, K. Yoshida, R. Oshima, Y. Shoji, T. Inoue, and T. Kita, J. Appl. Phys. **109**, 024301 (2011).
[14]J. Hwang, K. Lee, A. Teran, S. Forrest, J. D. Phillips, A. J. Martin, and J. Millunchick, Phys. Rev. Appl. **1**, 051003 (2014).
[15]T. Kada, S. Asahi, T. Kaizu, Y. Harada, T. Kita, R. Tamaki, Y. Okada, and K. Miyano, Phys. Rev. B **91**, 201303 (2015).
[16]T. Kada, S. Asahi, T. Kaizu, Y. Harada, R. Tamaki, Y. Okada, and T. Kita, Sci. Rep. **7**, 5865 (2017).
[17]Y. Shoji, R. Tamaki, and Y. Okada, AIP Adv. **7**, 065305 (2017).
[18]T. Kita, T. Maeda, and Y. Harada, Phys. Rev. B **86**, 035301 (2012).
[19]M. Yoshida, N. J. Ekins-Daukes, D. J. Farrell, and C. C. Phillips, Appl. Phys. Lett. **100**, 263902 (2012).
[20]S. Asahi, H. Teranishi, K. Kusaki, T. Kaizu, and T. Kita, Nat. Commun. **8**, 14962 (2017).
[21]S. Asahi, K. Kusaki, Y. Harada, and T. Kita, Sci. Rep. **8**, 872 (2018).
[22]S. Asahi and T. Kita, Nat. Commun. **10**, 956 (2019).
[23]N. Kinugawa, S. Asahi, and T. Kita, Phys. Rev. Appl. **14**, 014010 (2020).
[24]S. Asahi and T. Kita, in *Proceedings of the IEEE 46th Photovoltaic Specialists Conference* (IEEE, 2019), pp. 2597–2599.
[25]J. M. Woodall and H. J. Hovel, Appl. Phys. Lett. **21**, 379 (1972).
[26]R. Sahai and A. G. Milnes, Solid. State. Electron. **13**, 1289 (1970).
[27]P. D. Demoulin, M. S. Lundstrom, and R. J. Schwartz, Sol. Cells **20**, 229 (1987).
[28]F. A. J. M. Driessen, Appl. Phys. Lett. **67**, 2813 (1995).
[29]K. Yamashita, T. Kita, and T. Nishino, J. Appl. Phys. **84**, 359 (1998).
[30]T. Kita, T. Nishino, C. Geng, F. Scholz, and H. Schweizer, Phys. Rev. B **59**, 15358 (1999).
[31]M. A. Green, *Third Generation Photovoltaics* (Springer Berlin Heidelberg, 2006).
[32]P. Harrison, in *Quantum Wells, Wires Dots*, 2nd ed. (John Wiley & Sons, Inc., Chichester, 2005), pp. 332–338.
[33]D. Bimberg, M. Grundmann, and N. N. Ledentsov, in *Quantum Dot Heterostruct* (John Wiley & Sons, 1999), pp. 154–155.
[34]A. Takahashi, T. Ueda, Y. Bessho, Y. Harada, T. Kita, E. Taguchi, and H. Yasuda, Phys. Rev. B **87**, 235323 (2013).
[35]S. Birner, T. Zibold, T. Andlauer, T. Kubis, M. Sabathil, A. Trellakis, and P. Vogl, IEEE Trans. Electron Devices **54**, 2137 (2007).
[36]A. Trellakis, T. Zibold, T. Andlauer, S. Birner, R. K. Smith, R. Morschl, and P. Vogl, J. Comput. Electron. **5**, 285 (2006).
[37]I. Vurgaftman, J. R. Meyer, and L. R. Ram-Mohan, J. Appl. Phys. **89**, 5815 (2001).
[38]Z. Hameiri, L. Mai, and S. R. Wenham, Prog. Photovoltaics Res. Appl. **19**, 511 (2011).
[39]A. Lemaire, A. Perona, M. Caussanel, and A. Dollet, Microelectronics J. **101**, 104735 (2020).
[40]M. Grundmann, *The Physics of Semiconductors* (Springer International Publishing, Cham, 2016).
[41]K. R. McIntosh and C. B. Honsberg, Prog. Photovoltaics Res. Appl. **7**, 363 (1999).
[42]O. Breitenstein, P. Altermatt, K. Ramspeck, and A. Schenk, in *21st European Photovoltaic Solar Energy Conference* (WIP-Renewable Energies, Munich, 2006).
[43]O. Breitenstein, J. Bauer, A. Lotnyk, and J.-M. Wagner, Superlattices Microstruct. **45**, 182 (2009).
[44]K. C. Fong, K. R. McIntosh, and A. W. Blakers, Prog. Photovoltaics Res. Appl. **21**, 490 (2013).
[45]W. Tress, M. Yavari, K. Domanski, P. Yadav, B. Niesen, J. P. Correa Baena, A. Hagfeldt, and M. Graetzel, Energy Environ. Sci. **11**, 151 (2018).
[46]K. R. Mcintosh and C. B. Honsberg, in *16th European Photovoltaic Solar Energy Conference* (WIP-Renewable Energies, Munich, 2000).
[47]S. Steingrube, O. Breitenstein, K. Ramspeck, S. Glunz, A. Schenk, and P. P. Altermatt, J. Appl. Phys. **110**, 014515 (2011).
[48]A. Otaegi, V. Fano, N. Azkona, E. Cereceda, L. Pérez, P. Rodríguez, F. Recart, J. R. Gutiérrez, and J. C. Jimeno, AIP Conf. Proc. 2147, 020010 (2019).